J Therm Anal Calorim (2009) 97:559–564
DOI 10.1007/s10973-009-0075-7

Thermal and structural characterization of $SrTi_{1-x}Nd_xO_3$

Márcia R. S. Silva · Mary C. F. Alves · S. J. G. Lima · L. E. B. Soledade · Elaine C. Paris · E. Longo · A. G. Souza · Iêda M. G. Santos

Received: 25 September 2008 / Accepted: 24 February 2009 / Published online: 10 June 2009

Abstract $Sr(Ti,Nd)O_3$ was synthesized in order to evaluate the influence of the amount of neodymium on the thermal and structural properties of $SrTiO_3$. The synthesis was carried out using the polymeric precursor method. A small mass gain was observed for the $SrTiO_3$ and $SrTi_{0.98}Nd_{0.02}O_3$ samples accompanied by an exothermic peak in the DTA curves. Other steps at higher temperatures are assigned to the combustion of the organic material and carbonate. Elimination of defects by previous calcination of the precursors is responsible by the short and long range ordering of the perovskite. Cubic phase was obtained for undoped and doped $SrTiO_3$.

Keywords Thermal analysis · Perovskite · Neodymium

Introduction

Strontium titanate single crystal ($SrTiO_3$) shows important technological interest in the microelectronics industry, due to its high dielectric constant, good magnetic, ferroelectric and insulating properties, outstanding wear resistance, high resistance against oxidation, and high chemical and thermal stabilities [1]. Its structural properties are known to be temperature dependent, while its electrical, optical and magnetic properties can be modified by the incorporation of dopants [2]. $SrTiO_3$ perovskites doped with transition metal and rare earth ions have attracted much attention due to the useful properties of luminescence, photochromism and electronic conduction [3]. Furthermore, perovskite-structure materials are attractive as host matrices for rare earth doping because of their applications in integrate light-emission devices, field emissions display (FEDs), all-solid compact laser devices operating in the blue–green region and positive temperature coefficient (PTC) resistors [4].

In relation to its structure at room temperature $SrTiO_3$ is an ideal cubic perovskite, with lattice parameter a = 3.905 Å, space group *Pm3m*. The structure consists of corner-connected TiO_6 octahedra. The Ti cations are placed in the centers of the octahedral, whereas the O^{2-} anions are situated at their corners. The Sr^{2+} cations lie in the centers of the cavities formed by the TiO_6 octahedra network and are characterized by 12-fold O-coordination [5]. Below 105 K it adopts a tetragonal structure with space group *I4/mcm* [6].

In this work, samples of the $SrTi_{1-x}Nd_xO_3$(x = 0;0.01;0.02 and 0.04) system were synthesized in order to evaluate the influence of the amount of neodymium on the thermal and structural properties of the system. The synthesis was carried out by the polymeric precursor method [7], which presents several advantages such as: chemical homogeneity of multicomponent compounds at the molecular scale, direct and precise control of stoichiometry in complex systems at relatively low temperatures and simply way of manufacturing. Moreover, it has been widely used by our research group to synthesize various compounds with different structures [8–11] including $SrTiO_3$ [12].

M. R. S. Silva · M. C. F. Alves · L. E. B. Soledade · E. C. Paris · A. G. Souza · I. M. G. Santos (✉)
LACOM, Departamento de Química/CCEN, Universidade Federal da Paraíba, Campus I, João Pessoa, PB CEP 58059-900, Brazil
e-mail: ieda@quimica.ufpb.br

S. J. G. Lima
Laboratório de Solidificação Rápida/CT, UFPB, João Pessoa, PB, Brazil

E. Longo
CMDMC/LIEC/Instituto de Química, UNESP, Araraquara, SP, Brazil

Experimental

A titanium citrate solution was initially prepared as previously described [13]. During the synthesis citric acid was added to the titanium citrate solution at 90 °C. A 3:1 citric acid:metal molar ratio was used. After solubilization, neodymium oxide, Nd_2O_3 (Merck) and strontium nitrate (Vetec) were added to the solution, followed by ethylene glycol (Vetec) addition. A 60:40 citric acid:ethylene glycol mass ratio was used.

The polymeric resin was calcined at 300 °C for 30 min. After this first calcination, the powder precursors were submitted to milling in an alcoholic medium for 4 h in an attritor type mill. Another calcination was performed in an oxygen atmosphere at a flow rate of 2 mL min^{-1}, at 250 °C for 12 h. The precursors were de-agglomerated and calcined in oxygen at 300 °C for 12 h. In each step the powders were evaluated by using a SDT 2960 model Simultaneous DTA-TG from TA Instruments. The experiments were carried out from room temperature to 1000 °C in an air atmosphere with a flow rate of 110 mL min^{-1}, and at a heating rate of 10 °C min^{-1}. About 10 mg of samples were weighed in alumina crucibles.

The powder precursors were heat treated in air between 400 and 700 °C for 2 h. The infrared spectroscopy analyses were performed in a 3100 VARION spectrophotometer. The spectra using KBr pellets were recorded in the 2000–400 cm^{-1} range. The UV–VIS spectra were obtained in a UV-2550 Shimadzu spectrophotometer in the 190–900 nm range using reflectance mode. The structural transformations were evaluated by X-ray diffraction (D-5000 Siemens). The analyses were obtained with a 0.03° step and a step time of 1.0 s using the CuKα radiation. The sample heat treated at 700 °C was characterized by means of the Rietveld refinement of the XRD patterns. For this sample, the X-ray diffraction data were collected using a Rigaku DMax 2500PC diffractometer applying 40 kV and 150 mA with Cu Kα radiation, graphite monochromator and rotary anode. In the analysis a 2θ range from 10 up to 110° in a step-scanning mode was used, with step width of 0.02° s^{-1} and fixed time of 3 s. The divergence slit used was fixed at 1° and receiving slit at 0.3 mm. The Rietveld refinement for the sample heat treated at 700 °C was conducted by means of the (GSAS) package—General Structure Analysis System program of Larson and Von Dreele [14]. The peak profile function was modeled using a convolution of the pseudo-Voigt with the asymmetry function described by Finger [15].

Results and discussion

The thermogravimetric curves are presented in Fig. 1. Pure and doped $SrTiO_3$ powder precursors had three

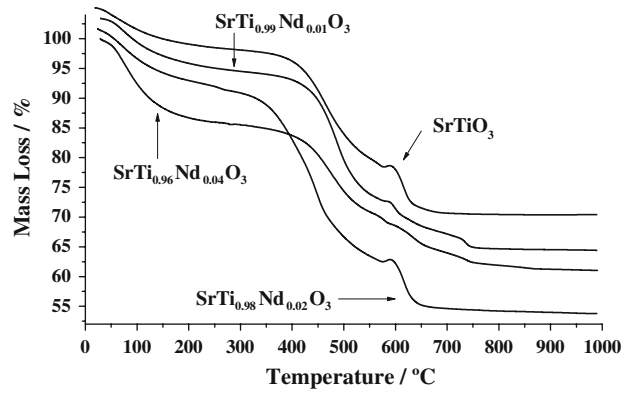

Fig. 1 TG curves of the powder precursors of $SrTi_{1-x}Nd_xO_3$

decomposition steps, except for the $SrTi_{0.99}Nd_{0.01}O_3$ and $SrTi_{0.96}Nd_{0.04}O_3$ precursors, which had one more step. Peaks assigned to the different steps were observed in the DTA curves (Fig. 2).

The thermogravimetric curves showed the first mass loss step at low temperatures, being assigned to the elimination of water and gases adsorbed on the surface of the powders. Other steps at higher temperatures are assigned to the combustion of the organic material. Their amounts increased with the neodymium addition, but when $x = 0.04$ they decrease as observed in Table 1.

A small mass gain was observed for $SrTiO_3$ (0.18%) and $SrTi_{0.98}Nd_{0.02}O_3$ (0.06%) samples at about 583 °C, associated with an exothermic peak in the DTA curve. This kind of transition is usually assigned to oxidation reactions. In the present work it seems that the Ti^{4+} reduction occurred at an earlier stage of the thermal treatment leading to the formation of oxygen vacancies as showed in Eq. 1 written using the Kroger Vink notation [16]. At higher temperatures, the oxidation of Ti^{2+} took place with oxygen

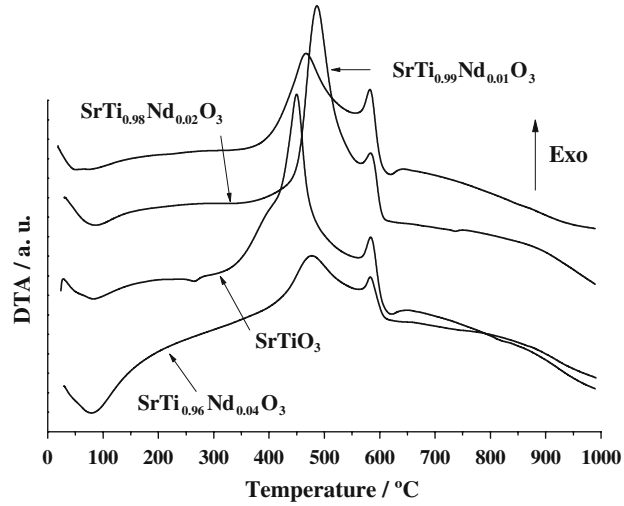

Fig. 2 DTA curves of the powder precursors of $SrTi_{1-x}Nd_xO_3$

Table 1 Elimination of organic matter

Sample	Second step		Third step	
	DTG peak temperature (°C)	Δm (%)	DTG peak Temperature (°C)	Δm (%)
$SrTiO_3$	464	19.5	–	–
$SrTi_{0.99}Nd_{0.01}TiO_3$	487	21.5	599	5.23
$SrTi_{0.98}Nd_{0.02}TiO_3$	448	28.2	–	–
$SrTi_{0.96}Nd_{0.04}TiO_3$	475	17.7	577	1.92

absorption leading to the mass gain associated to the exothermic transition.

$$TiO \rightarrow Ti''_{Ti} + V^{\cdot\cdot}_{O} + O^{x}_{O} \quad (1)$$

The last mass loss step was observed above 600 °C being associated with an endothermic peak in the DTA curves. This transition was assigned to the carbonate decomposition as strontium carbonate is easily formed when organic material is present. The carbonate decomposition finished at different temperatures depending on the amount of dopant; at 782 °C for $SrTiO_3$, 803 °C for $SrTi_{0.99}Nd_{0.01}O_3$,

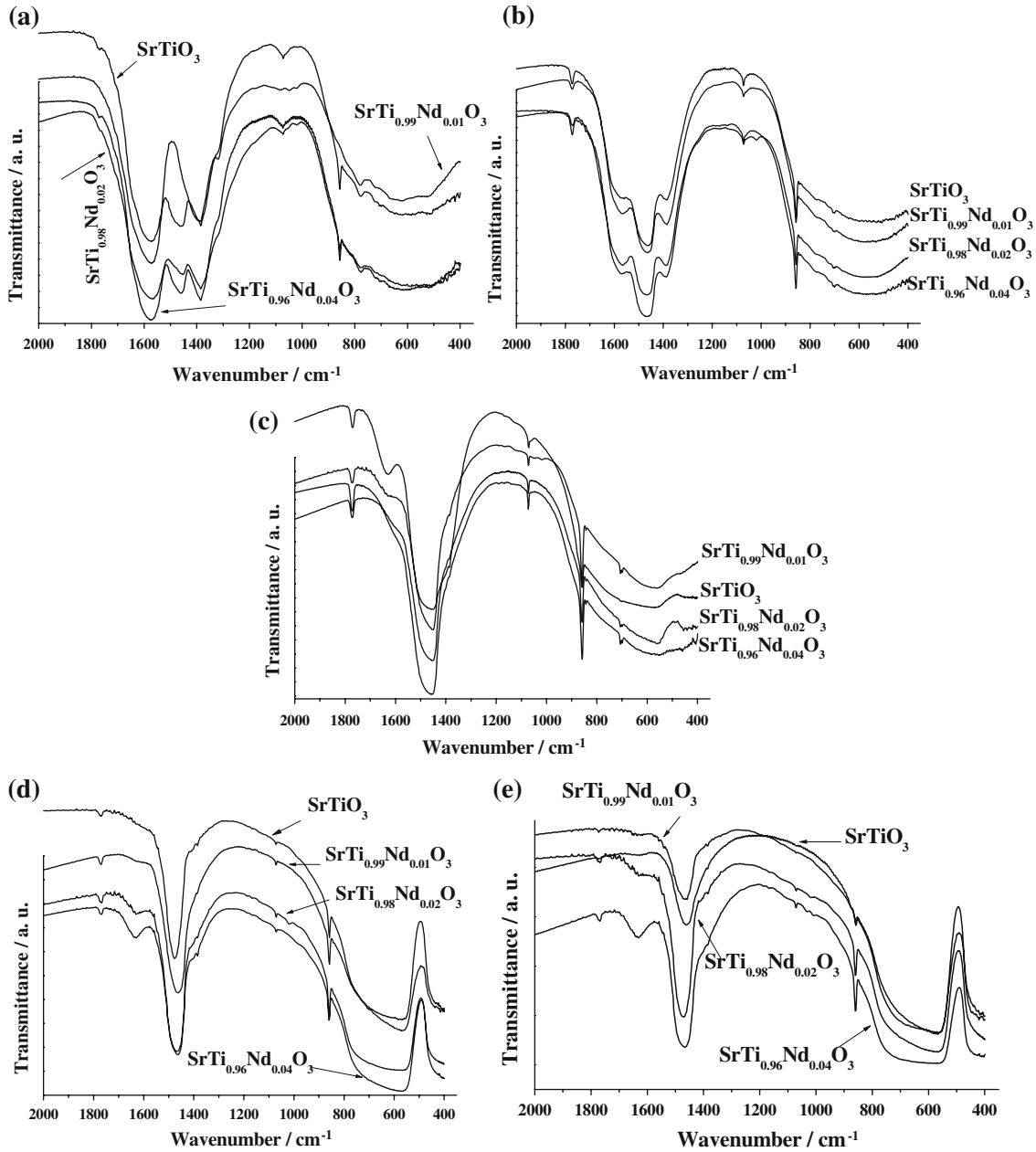

Fig. 3 Infrared spectra of the powder precursor calcined at different temperatures: **a** 300 °C, **b** 400 °C, **c** 500 °C, **d** 600 °C and **e** 700 °C

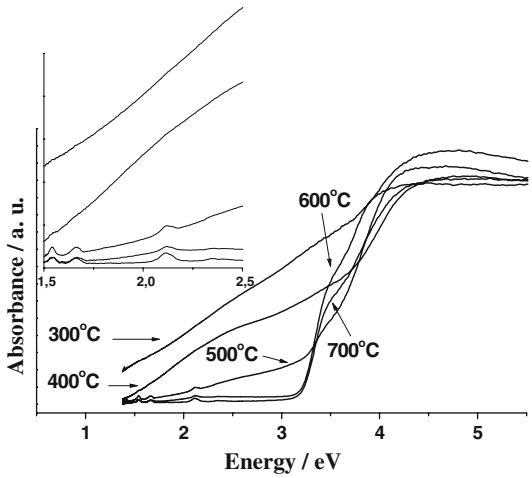

Fig. 4 UV–VIS spectra of $SrTi_{0.99}Nd_{0.01}O_3$, calcined between 300 and 700 °C. *Insert* Detail of spectra, showing Nd^{3+} transitions

749 °C for $SrTi_{0.98}Nd_{0.02}O_3$ and 900 °C for $SrTi_{0.96}Nd_{0.04}O_3$.

The infrared spectra are showed in Fig. 3. The presence of organic material and carbonates was confirmed by the bands at 1770, 1580, 1460, 1384, 1070, 860 and 700 cm^{-1}. The bands at 1580 and 1384 cm^{-1} were assigned to the presence of esters [17]. The intensities of these bands decreased continuously up to 500 °C (Fig. 3c), indicating that the second and third mass loss steps in TG curves are due to the combustion of these esters. The bands at 1770, 1460, 1384 (superposed to the ester bands), 1070, 860 and 700 cm^{-1} were assigned to the presence of carbonates [18, 19]. The decrease in the intensity of these bands only occurred after calcination at 700 °C (Fig. 3e), confirming the TG/DTA data. The higher amount of neodymium doping made the carbonate elimination more difficult. One

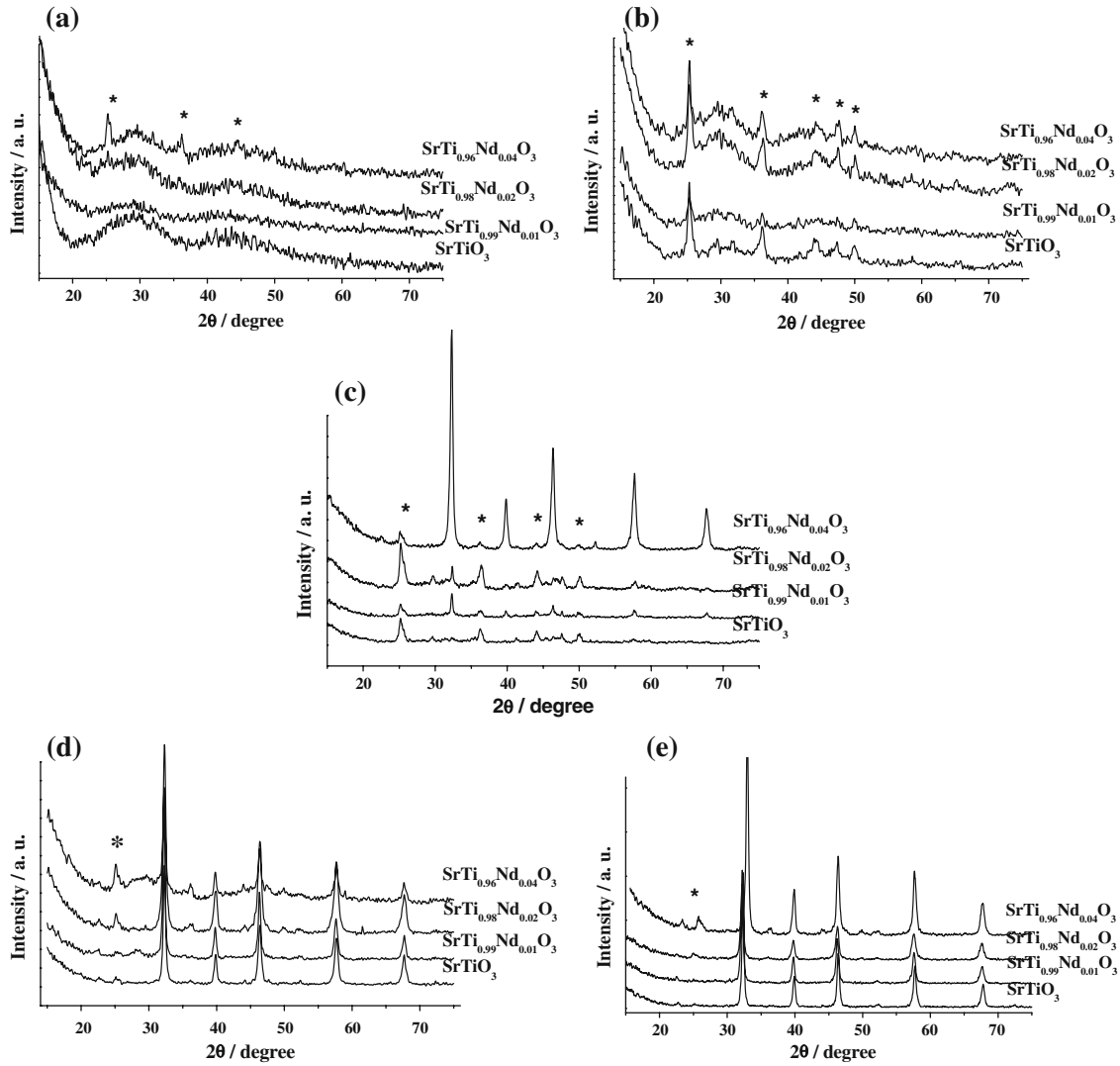

Fig. 5 XRD patterns of the $SrTi_{1-x}Nd_xO_3$ samples calcined at different temperatures: **a** 300 °C, **b** 400 °C, **c** 500 °C, **d** 600 °C and **e** 700 °C. Legend: (*) $SrCO_3$. Peaks that are not indexed are assigned to the perovskite phase

band assigned to water was observed at 1630 cm^{-1} for the neodymium doped samples, after calcination at 500 °C.

The metal-oxygen band was observed below 800 °C. This band was very broad and with low definition after calcination at 300 and 400 °C (Fig. 3a, b), indicating that the samples were short-range disordered. Neodymium addition favored the short range ordering, after calcination at 500 °C being possible to observe two broad bands. The first one between 800 and 550 cm^{-1} and the second one below 500 cm^{-1}. A higher definition of these bands was observed for all samples after calcination at 600 °C (Fig. 3d).

According to the UV–VIS spectra (Fig. 4), the powders calcined below 500 °C displayed a small absorption below 3 eV, which disappeared after calcination at 600 °C. This fact was related to the defect formation. At low temperature the defects were deeper into the band gap leading to electronic transitions of smaller energies. When temperature increased, the defects were eliminated and these transitions were no longer observed. It seems that these defects could be oxygen vacancies as suggested in the thermal analysis results, which showed a mass gain at 583 °C.

An important point in the UV–VIS spectra was the presence of Nd^{3+} peaks between 1.5 and 2.5 eV. These peaks were only observed after calcination above 500 °C probably due to the short range ordering of the NdO_6 polyhedra as already observed in the IR spectra.

The XRD patterns (Fig. 5) showed that perovskite only crystallized above 500 °C. The orthorhombic strontium carbonate was observed in all temperatures with a decrease in its intensity after calcination at 700 °C. The Rietveld results indicated that only 2.9% in mass of $SrCO_3$ was present at this temperature.

In relation to the perovskite crystallization the cubic phase was obtained but there are indications of the presence of the tetragonal $SrTiO_3$. This observation still needs to be confirmed with the aid of other techniques. Neodymium addition into the $SrTiO_3$ lattice favored the ordering at 500 °C but also favored the formation of carbonate phase at 300 °C, as clearly observed for the $SrTi_{0.96}Nd_{0.04}O_3$ sample.

Conclusions

The thermogravimetric curves showed four mass variation steps, which were identified with the aid of other techniques as infrared spectroscopy and UV-VIS spectroscopy. The mass loss steps between 200 and 580 °C were assigned to ester combustion, while the step above ~600 °C was assigned to carbonate decomposition. The mass gain was assigned to oxygen absorption, with Ti^{2+} oxidation and defects elimination. The previous heat treatment of the precursors in oxygen atmosphere made carbonate elimination easier so that only 2.9 mass% of $SrCO_3$ remained in the undoped sample calcined at 700 °C. A higher amount of neodymium made perovskite crystallization easier in spite of the higher difficulty in the elimination of the carbonate.

Acknowledgements The authors thank to CNPq/MCT, Proinfra/FINEP, CEPID/FAPESP and CAPES for the financial support to this work.

References

1. Zhang Y, Lian J, Wang CW, Jiang W, Ewing RC, Weber WJ. Ion-induced damage accumulation and electron-beam-enhanced recrystallization in $SrTiO_3$. Phys Rev B. 2005;72:094112.
2. Marques AC, Correia JG, Wahl U, Soares JC. Study of point defects and phase transitions in undoped and Nb-doped $SrTiO_3$ using perturbed angular correlations. Nucl Instrum Methods Phys Res Sect B. 2007;261:604–7.
3. Wen-Chen Z, Hong-Gang L, Gu-Ming J, Lv H. Spin-Hamiltonian parameters and local structures for Co^{4+} and Ir^{4+} impurity centers in the tetragonal phase of $SrTiO_3$. Spectrochim Acta A. 2008;71:1551–4.
4. Samantaray CB, Nanda-Goswami ML, Bhattacharya D, Ray SK, Acharya HN. Photoluminescence properties of Eu^{3+}-doped barium strontium titanate (Ba, Sr)TiO_3 ceramics. Mater Lett. 2004;58:2299–301.
5. Levin AA, Paufler P, Meyer DC. Low-temperature domain behaviour of a $SrTiO_3$ (0 0 1) single-crystal plate. Physica B. 2007;393:373–81.
6. Ikeda T, Kobayashi T, Takata M, Takayama T, Sakata M. Charge density distributions of strontium titanate obtained by the maximum entropy method. Solid State Ionics. 1998;108:151–7.
7. Leite ER, Sousa CMG, Longo E, Varela JA. Influence of polymerization on the synthesis of $SrTiO_3$: Part I: characteristics of the polymeric precursors and their thermal decomposition. Ceram Int. 1995;21:143–52.
8. de Oliveira ALM, Ferreira JM, Silva MRS, Braga GS, Soledade LEB, Maurera MAMA, et al. Yellow $Zn_xNi_{1-x}WO_4$ pigments obtained using a polymeric precursor method. Dyes Pigm. 2008;77:210–6.
9. Silva MRS, de O'Miranda LC, Cássia-Santos MR, Lima SJG, Soledade LEB, Longo E, et al. Influence of the network former on the properties of magnesium spinels. J Therm Anal Cal. 2007;87:753–7.
10. Alves MCF, Souza SC, Lima SJG, Longo E, Souza AG, Santos IMG. Influence of the precursor salts in the synthesis of $CaSnO_3$ by the polymeric precursor method. J Therm Anal Cal. 2007;87:763–6.
11. Melo DS, Marinho EP, Soledade LEB, Melo DMA, Lima SJG, Longo E, et al. Lanthanum-based perovskites obtained by the polymeric precursor method. J Mater Sci. 2007;43:551–6.
12. Silva MRS, Soledade LEB, Lima SJG, Longo E, Souza AG, Santos IMG. Influence of processing conditions on the thermal decomposition of $SrTiO_3$ precursors. J Therm Anal Cal. 2007;87:731–5.
13. Silva MRS, Souza SC, Santos IMG, Cássia-Santos MR, Soledade LEB, Souza AG, et al. Stability studies on undoped and doped Mg_2TiO_4, obtained by the polymeric precursor method. J Therm Anal Cal. 2005;79:421–4.

14. Rietveld HM. A profile refinement method for nuclear and magnetic structures. J Appl Cryst. 1969;2:65–71.
15. Finger LW, Cox LW, Jephcoat DE. A correction for powder diffraction peak asymmetry due to axial divergence. J Appl Cryst. 1994;27:892–900.
16. Chiang IM, Kingery WD, Birnie DP. Physical ceramics—principle for ceramic science and engineering. New York: Wiley; 1997. p. 110.
17. Nakamoto K. Infrared and Raman spectra of inorganic and coordination compounds. New York: Wiley; 1980. p. 232.
18. Nyquist RA, Kagel RO. Infrared spectra of inorganic compounds. San Diego: Academic Press; 1971. p. 78.
19. Suasmoro S, Pratapa S, Hartanto D, Setyoko D, Dani UM. The characterization of mixed titanate $Ba_{1-x}Sr_xTiO_3$ phase formation from oxalate coprecipitated precursor. J Eur Ceram Soc. 2000;20:309–14.